



pubs.acs.org/JACS Article

Non-Covalent Interactions Mimic the Covalent: An Electrode-Orthogonal Self-Assembled Layer

Deepak Badgurjar, Madison Huynh, Benjamin Masters, and Anna Wuttig*



Cite This: J. Am. Chem. Soc. 2023, 145, 17734–17745



Read Online

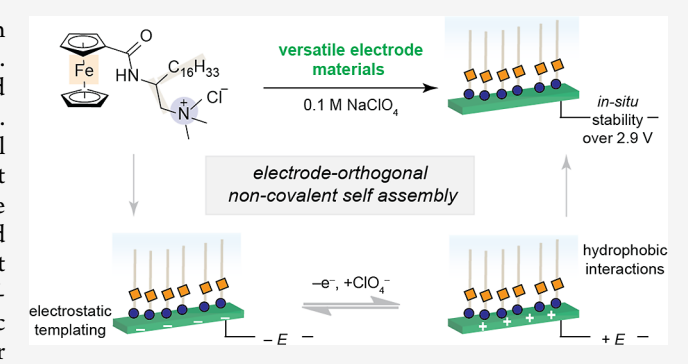
ACCESS I

III Metrics & More

Article Recommendations

s Supporting Information

ABSTRACT: Charge-transfer events central to energy conversion and storage and molecular sensing occur at electrified interfaces. Synthetic control over the interface is traditionally accessed through electrode-specific covalent tethering of molecules. Covalent linkages inherently limit the scope and the potential stability window of molecularly tunable electrodes. Here, we report a synthetic strategy that is agnostic to the electrode's surface chemistry to molecularly define electrified interfaces. We append ferrocene redox reporters to amphiphiles, utilizing non-covalent electrostatic and van der Waals interactions to prepare a self-assembled layer stable over a 2.9 V range. The layer's voltammetric response and *in situ* infrared spectra mimic those reported for



analogous covalently bound ferrocene. This design is electrode-orthogonal; layer self-assembly is reversible and independent of the underlying electrode material's surface chemistry. We demonstrate that the design can be utilized across a wide range of electrode material classes (transition metal, carbon, carbon composites) and morphologies (nanostructured, planar). Merging atomically precise organic synthesis of amphiphiles with *in situ* non-covalent self-assembly at polarized electrodes, our work sets the stage for predictive and non-fouling synthetic control over electrified interfaces.

■ INTRODUCTION

Covalent bond formation between molecules and electrode surfaces serves as a predominant synthetic strategy to molecularly define the structure of electrified interfaces. For example, by leveraging the robust metal-sulfur bond, 1-3 redoxactive or field-sensitive reporters containing a thiol precursor can be installed at an electrode surface (Scheme 1, left). This synthetic approach has been used to answer key mechanistic questions in energy conversion and storage, biomolecular sensing, and electronic devices, such as the electron transfer properties of biomolecules, 4,5 interfacial acid-base equilibria, 6-8 and the directionality of electron transfer reactions, 9,10 as well as enabling new modalities to enhance electrochemical reactivity, 11-13 among numerous other advances. However, the reliance of specific covalent bond-forming events (e.g., using thiol, isocyanide, and carbene precursors)^{14–17} on select metal surfaces (Au, Pd, Pt, Cu, Ag, and Hg) precludes generalizability across: (1) a wider range of electrode materials and (2) applied potentials due to competitive oxidative and reductive desorption. While the use of $\pi-\pi$ stacking of pyrene with carbon electrodes or diazonium grafting onto electrode surfaces has enabled systematic and tunable modifications,^{23–29} these linkages are specific to their underlying electrode material and exhibit competitive potentialdependent desorption, electropolymerization, or multilayer formation. The identification of new material compositions for electrochemical applications, namely, non-precious

metal and metal-free electrodes, necessitates a general synthetic technology that is independent of the potential-dependent linkage stability *in situ*. Such a strategy would enable us to molecularly define the structure of the electrified interface without irreversibly modifying the electrode itself; this electrode-orthogonal approach would be agnostic to the surface chemistry of the electrode material yet retain the modular and predictive nature of covalent synthetic strategies.

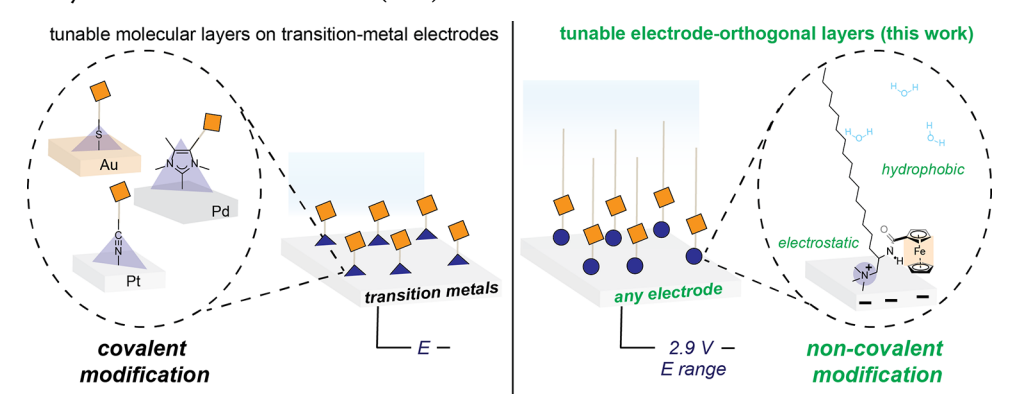
The addition of amphiphiles to electrochemical systems is known to modulate key charge-transfer events. 30,34-40 It is theorized that these charge-transfer events are driven by the non-covalent electrostatic attraction of the charged amphiphile to the oppositely charged electrode surface, which creates a hydrophobic pocket. 41-44 This self-assembly has been posited to be potential-dependent, 41,43-45 e.g., for a cationic amphiphile, the structure is formed negative of the potential of zero free charge (PZFC, the potential at which the interfacial field is the weakest). Yet, this mechanistic model cannot explain prior work that suggests that cationic

Received: April 27, 2023 Published: August 7, 2023



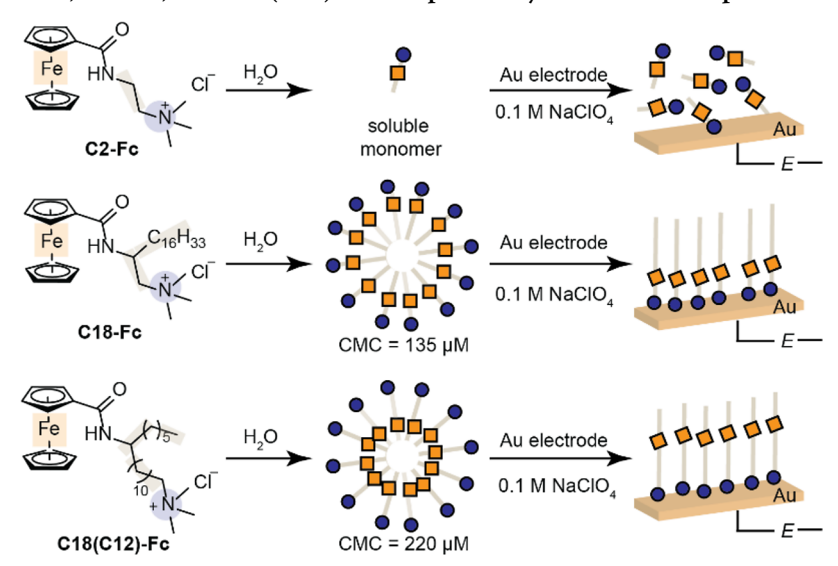


Scheme 1. Predominant Synthetic Strategy to Produce Molecularly Tunable Layers on Electrodes Utilize Covalent Interactions to Modify Transition-Metal Surfaces (Left)^a



^aThis work describes an alternative, non-covalent approach for modification of a diverse array of electrode materials, yielding electrochemical charge-transfer properties that mimic those of covalently modified systems over an expanded 2.9 V range. The electrode-orthogonal layer (right) is easily removed by rinsing with water.

Scheme 2. Summary of C2-Fc, C18-Fc, and C18(C12)-Fc Compounds Synthesized and Supramolecular Aggregates Thereof



"Micelles formed in the bulk aqueous solution (middle). Charge-balancing anions omitted for clarity. Simplified schematic of proposed interfacial structure upon contact with charged polycrystalline Au working electrode in aqueous electrolytes (right). Water, charge-balancing anions, and possible structural disorder of aliphatic chains omitted for clarity.

amphiphiles are still positioned at the polarized interface at potential values where electrostatic repulsion should repel them (i.e., applied potential values are far positive of the PZFC).⁴² Thus, we hypothesized that non-covalent van der Waals interactions between aliphatic chains of the amphiphile could override electrostatic repulsion.

Here, we reveal that the combination of non-covalent electrostatic and van der Waals interactions enables the formation of a self-assembling molecular layer. We report that the latter non-covalent interaction enables the layer to remain intact even at applied potential values where electrostatic repulsion should repel the layer. We append a ferrocene (Fc) redox reporter onto a series of cationic amphiphiles with varying aliphatic chains to enable us to track and quantify layer formation. We leverage this insight in a synthetic strategy to produce self-assembled electrode-orthogonal layers at electrode interfaces that are stable over an expanded potential range (Scheme 1, right). As the layer is formed solely due to non-covalent interactions, self-assembly occurs on a wide array

of electrode material compositions without permanent surface structural changes, i.e., the layer is removed by rinsing the electrode with water and can be restored by reintroduction of the amphiphile to the electrolyte. The in situ self-assembled layer is maintained in electrolytes that contain the amphiphile over potential ranges from -1.8 to 1.1 V vs Ag/AgCl, a window 0.9 V wider than the potential stability range of covalent linkers^{18–22} and 0.3 V greater than existing noncovalent^{23,29} linkers.

RESULTS AND DISCUSSION

Structure-Dependent Ferrocene Redox Features Observed in the Absence of Covalent Tethering. To track and quantify layer formation, we appended a ferrocene (Fc) redox reporter to cationic amphiphiles. Scheme 2 summarizes the synthesized probes (see Supporting Information (SI), for details): (1) C2-Fc, a control monomer without a long aliphatic chain; (2) C18-Fc, a monomer containing a long aliphatic chain with the Fc moiety close to the

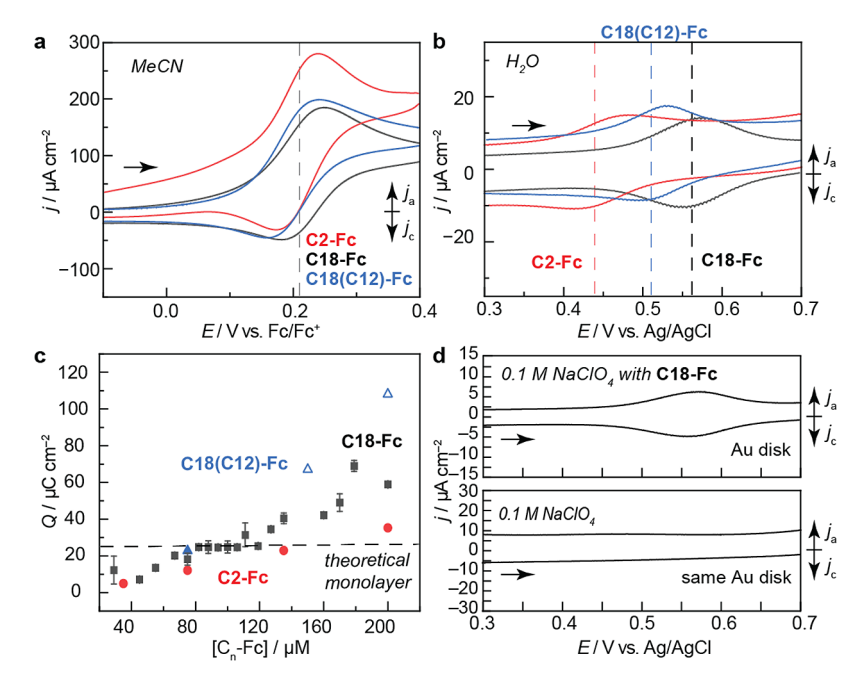


Figure 1. Electrochemical response of C2-Fc, C18-Fc, and C18(C12)-Fc in varying electrolyte media. (a) CV of 1 mM C2-Fc (red), 1 mM C18(C12)-Fc (blue), or 1 mM C18-Fc (black) in 0.1 M TBAClO₄ in MeCN collected at 50 mV s⁻¹ on a Au working disk electrode. (b) CV of 75 μM C2-Fc (red), 75 μM C18(C12)-Fc (blue), or 75 μM C18-Fc (black) in 0.1 M NaClO₄ in H₂O collected at 50 mV s⁻¹ on a Au working disk electrode. Dashed lines in panels a and b estimate the $E_{1/2}$ of the reversible CV waves observed. (c) Charge integration of the Fc anodic redox in 0.1 M NaClO₄ for data collected on a Au disk electrode for C18-Fc (black squares, error bars represent the average and range of 2–3 independent runs), C18(C12)-Fc (blue diamonds, where open blue diamond data points are convoluted with C18(C12)-Fc precipitation), and C2-Fc (red circles). The calculated theoretical charge for a monolayer of C18-Fc is indicated by the black dashed line. (d) Rinse test of C18-Fc in an aqueous electrolyte. (Top) CV of 200 μM C18-Fc in 0.1 M NaClO₄ in H₂O collected at 20 mV s⁻¹ on a Au disk working electrode. (Bottom) CV of the same Au working electrode as the (top) in 0.1 M NaClO₄ in H₂O that immediately follows rinsing of the Au electrode in H₂O. CV collected at 20 mV s⁻¹. All CVs collected with a positive direction of scan under N₂ atmosphere.

ammonium; and (3) C18(C12)-Fc, a monomer containing an identical aliphatic chain but with the Fc moiety positioned further away from the cationic group. We determined each monomer's critical micelle concentration (CMC) and surface tension (Scheme 2, middle, Table S1, Table S2, Figures S1 and S2). These results demonstrate that the hydrophobic interactions induced by the presence of the long alkyl chains serve as the primary non-covalent interaction to drive supramolecular aggregate formation in aqueous solution at μ M quantities, Scheme 2, middle.

The redox features of C2-Fc, C18-Fc, and C18(C12)-Fc are nearly identical in nonaqueous media and indicative of diffusion-controlled and reversible single-electron transfer. We chose Au disk electrodes to enable interfacial structural characterization via surface-enhanced infrared absorption spectroscopy (SEIRAS), see below. Figure 1a depicts the cyclic voltammogram (CV) of C2-Fc (red), C18-Fc (black), and C18(C12)-Fc (blue) in acetonitrile (MeCN) containing 0.1 M tetrabutylammonium perchlorate (TBAClO₄). We chose ClO₄⁻ because studies show that the reversibility of the Fc redox wave is dependent on the electrolyte anion and is most preserved in the presence of ClO₄-.46-48,52 For all molecules examined, near-identical redox features centered at an anodic peak potential value, E_{pa} , of 232–245 mV vs Fc/Fc⁺ and a cathodic peak potential, $E_{\rm pc}$, value of 170–185 mV vs Fc/Fc^{+} are observed. Following, the redox potentials $(E_{1/2})$ lie at 210 \pm 5 mV vs Fc/Fc⁺ (gray, Figure 1a). The peak potential separation between E_{pa} and E_{pc} is 60 mV, indicative of diffusion-controlled and reversible single-electron transfer. 49 Diffusion coefficients for C2-Fc, C18-Fc, and C18(C12)-Fc

are similar (Figure S3). These results indicate that, in nonaqueous media, C2-Fc, C18-Fc, and C18(C12)-Fc exist in a monomeric, solution-dissolved form, where changes in the aliphatic structure minimally impact the structure at the electrified Au interface (key electrochemical data summarized in Table S3).

In contrast, the redox behaviors of the molecules are drastically different in aqueous electrolytes and mimic those previously reported for covalently bound ferrocene at varying distances from the electrode surface. Figure 1b shows the CV of C2-Fc (red), C18-Fc (black), and C18(C12)-Fc (blue) in 0.1 M NaClO₄. For C2-Fc, we observe E_{pa} at 0.472 V vs Ag/ AgCl (all aqueous reference potentials quoted vs Ag/AgCl with resistance correction, Figure S4) and $E_{\rm pc}$ at 0.418 V ($E_{1/2}$ = 0.445 V, Figures 1b and S5), exhibiting a peak-to-peak separation of \sim 60 mV ($\Delta E_{\rm p} = E_{\rm pa} - E_{\rm pc}$) that remains constant at varying scan rates (Figure S6). These results are indicative of freely diffusive C2-Fc species in a monomeric form (Scheme 1, right). However, the $E_{1/2}$ value for C18(C12)-Fc exhibits a ~67 mV positive shift from the redox wave observed for C2-Fc $(E_{pa} \text{ at } 0.525 \text{ V and a } E_{pc} \text{ at } 0.499 \text{ V}, E_{1/2} = 0.512 \text{ V}, \text{ Figures 1b}$ and S7). This reproducible shift (Figure S8 and Table S4) is in line with previous work on covalently bound ferrocenylalkane thiols to Au electrodes, separating the Fc by six methylene units or more away from the S-Au linkage. 46,47,51 In these covalent systems, the positive Fc redox potential shifts are attributed to a potential drop of the Fc in the interfacial layer of low dielectric strength induced by the alkane matrix bound to Au. $^{46,47,50-52}$ In addition, a small $\Delta E_{\rm p}$ value of 26 mV is observed. This value is inconsistent with the 60-mV value

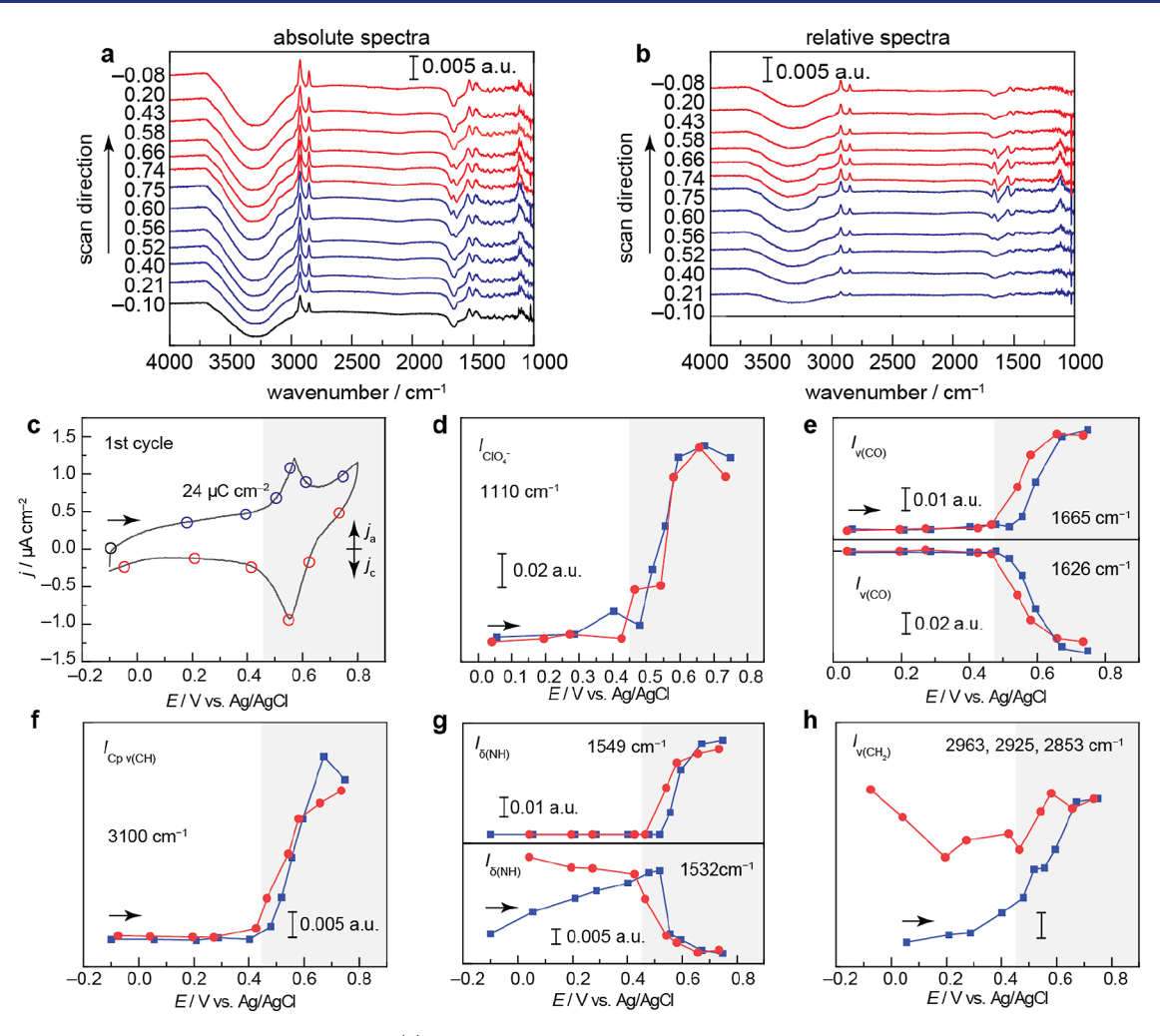
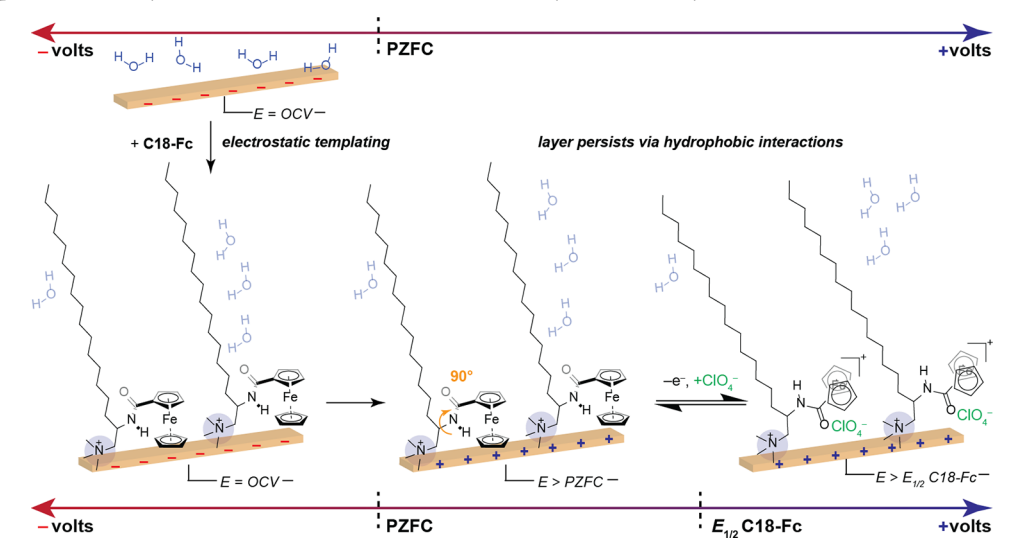


Figure 2. Spectroscopic data of self-assembled layer. (a) SEIRA spectra collected on the first CV cycle at the potential values indicated, where the background spectrum was collected at -0.1 V vs Ag/AgCl in 0.1 M NaClO₄ in the absence of 200 μM C18-Fc. (b) Identical spectra as shown in as a, however, the background spectrum was collected at -0.1 V vs Ag/AgCl in 0.1 M NaClO₄ in the presence of 200 μM C18-Fc. (c) The initial, first CV cycle collected upon the addition of 200 μM C18-Fc in tandem with a and b at 2 mV s⁻¹ from -0.1 V vs Ag/AgCl. The anodic integrated charge is shown. (d) Integrated band intensity (IBI) taken from b of the peak centered at 1110 cm⁻¹. (e) IBI taken from b of the peak centered at 1626 cm⁻¹. (f) IBI taken from b of the peak centered at 2963, 2925, and 2853 cm⁻¹.

expected for the single-electron redox signal associated with a diffusing species (or its micelle form),53 suggesting that C18(C12)-Fc organizes to form an immobilized structure at the electrode surface that positions the Fc units within an aliphatic matrix. This hypothesis is supported by the linearity expected and observed between the anodic (j_{pa}) and cathodic (j_{pc}) peak current with the CV scan rate, v_r (Figure S9) for surface-adsorbed redox-active species.⁵⁴ For C18-Fc, we observe $E_{\rm pa}$ at 0.566 V and $E_{\rm pc}$ at 0.559 V ($E_{1/2}$ = 0.563 V), exhibiting a small $\Delta E_{\rm p}$ value of 7 mV, and a 51 mV shift more positive from the redox wave observed for C18(C12)-Fc (Figure 1b, black, Figures S10 and S11). The small ΔE_p value (7 mV) observed for C18-Fc together with the linearity observed for j_{pa} and j_{pc} with v (Figure S9) is consistent with those reported for Fc covalently bound to Au electrode surfaces via thiol linkers separating the Fc by one or two methylene units from the S-Au linkage. 55,58 As previous work demonstrates that the positive $E_{1/2}$ redox shifts of covalently bound ferrocenylalkane thiols track the position of Fc placed inside the bound alkane layer with low dielectric strength, 46,47,50,51 the increase in $E_{1/2}$ for C18-Fc relative to C18(C12)-Fc further demonstrates that the Fc tethered to the long alkyl chain is in regions of lower dielectric strength than C18(C12)-Fc (key electrochemical data summarized in Table S5). The decrease in the normalized double layer capacitance (Figure S5) from data collected in C2-Fc, Figure 1b (red) to C18(C12)-Fc (blue) and C18-Fc (black) further supports the formation of a unique structure around the electrified Au with lower dielectric strength. Together, these electrochemical features in aqueous media are consistent with a structural model where the presence of a long aliphatic chain leads to the formation of immobilized structures with the ammonium head group pointing toward the Au surface, Scheme 2, right, on the timescale of the electrochemical measurement.

Charge integration of the Fc redox wave is consistent with monolayer formation. Ferrocene-terminated thiol monolayers on Au have been estimated to be correlated with a charge integration of \sim 43 μ C cm⁻². $^{52,62-66}$ This theoretical value is determined by taking the radius of ferrocene⁶⁷ and assuming a densely packed monolayer. The hypothetical charge integration for the C18-Fc monolayer is \sim 24 μ C cm⁻² (see SI, Table S6 and Figure S12). Indeed, we observe that the charge

Scheme 3. Proposed Asembly and Structure of Self-Assembled Layer Driven by Non-Covalent Interactions^a



"At the open circuit voltage (OCV), which is negative of the potential of zero free charge (PZFC) of polycrystalline Au, the addition of C18-Fc results in the formation of a layer due to electrostatic attraction between the cationic group and the negatively polarized electrode. Upon the application of oxidative potential $(E > Fc/Fc^+)$, the oxidized C18-Fc ion pairs with the perchlorate anion, resulting in a rotation around the $C(sp^3)$ - $N(sp^3)$ bond and a tilting of the aliphatic unit toward the interface. After the initial application of potential, the layer persists for multiple CV cycles at oxidizing potentials due to favorable hydrophobic interactions between the alkyl chains.

integration for the Fc redox wave plateaus at ~24 μ C cm⁻² for C18-Fc at Au disk electrodes for CV experiments conducted in the presence of C18-Fc between 67 and 119 μ M (Figure 1c, black). At higher concentrations of C18-Fc in solution, the charge integration increases, suggesting multilayer formation. This charge integration is different from that observed for freely diffusing C2-Fc, which rises linearly with increasing bulk solution concentration (Figure 1c, red) and consistently exhibits lower integrated values. We note that the investigation of a similar charge integration relationship for C18(C12)-Fc is convoluted by solubility limitations in the presence of 0.1 M NaClO₄ (Figure 1c, blue). Therefore, we cannot conclude that monolayer formation occurs on C18(C12)-Fc. Together, these results suggest that C18-Fc forms a monolayer at the electrified Au interface.

The data are consistent with non-covalent binding of C18-Fc to Au electrode surfaces. Figure 1d (top) demonstrates the redox feature for C18-Fc observed on a freshly annealed Au electrode surface. Subsequent scans of the Au electrode in the presence of C18-Fc alter neither the position nor the shape of the CV feature (Figure S13), demonstrating that the immobilized structure formed is stable over the timescale of the experiment. Following, the Au electrode was rinsed in water and then introduced to an electrolyte solution that does not contain C18-Fc. The resultant CV, Figure 1d (bottom), shows a featureless CV, demonstrating that C18-Fc is not covalently bound to the Au surface and that the layer can be removed by rinsing the electrode with water. The reintroduction of C18-Fc to this new electrolyte solution restores the redox feature (Figure S14). These results highlight that layer formation and maintenance involves the presence of a micromolar concentration of C18-Fc in the bulk solution lower than or near our measured CMC values (see Table S1). Indeed, our observation is consistent with literature reports on commercially available surfactants, where surface aggregate formation (hemimicelles) at a non-electrified solid/liquid interface occurs at surfactant bulk concentration values less

than or near the reported CMC values.^{68–70} Together, our data point to a self-assembly mechanism of the C18-Fc layer at the electrified Au interface that occurs in the absence of covalent bond formation and in the presence of C18-Fc in the bulk solution at micromolar concentrations, Scheme 2, right.

Spectroelectrochemical Data Consistent with Self-**Assembled Structure.** SEIRA spectra are consistent with the formation of a self-assembled C18-Fc layer at Au. SEIRAS utilizes nanostructured electrode surfaces to enhance IR absorption of molecules with transition dipole moments perpendicular to the surface. 71,72 Figure 2c depicts the CV of C18-Fc collected using a SEIRAS-active Au film (electrochemically active surface area characterized and compared to the Au disk in Figure S15).^{73,74} We observe a near-identical redox feature to that observed on the Au disk electrode, see above ($E_{1/2}$ at 0.562 V). We calculate an integrated charge (24 μ C cm⁻²) value identical to that estimated for monolayer coverage. These results indicate that, despite the difference in the preparation of Au films required for SEIRAS studies (nanostructured) and the higher C18-Fc solution concentration utilized for the spectroscopic measurements (200 μ M), the current-voltage profile and the surface population of C18-Fc are identical to that observed on Au disks.

Figure 2a depicts the SEIRA spectra collected during the CV scan in Figure 2c. The background spectrum was collected at $-0.10~\rm V$ (the open circuit voltage, OCV) in the absence of C18-Fc. Upon the addition of C18-Fc, significant spectroscopic changes are observed (Figure 2a, black, $-0.10~\rm V$). We observe a bleach at 3308 and 1668 cm $^{-1}$, attributed to the $\nu(\rm OH)$ stretching and $\delta(\rm HOH)$ bending modes of interfacial water. These results demonstrate that the addition of C18-Fc to the electrolyte expels interfacial water. We observe a rise at 2963, 2925, and 2853 cm $^{-1}$, attributed to the $\nu_{\rm sym}$ (N-CH $_3$) of the ammonium group, $\nu_{\rm as}$ (CH $_2$) and $\nu_{\rm sym}$ (CH $_2$) of the aliphatic tail in an all-trans configuration, respectively. These $\nu_{\rm as}$ (CH $_2$) and $\nu_{\rm sym}$ (CH $_2$) values are in line with reported values for covalently bound alkanethiol monolayers

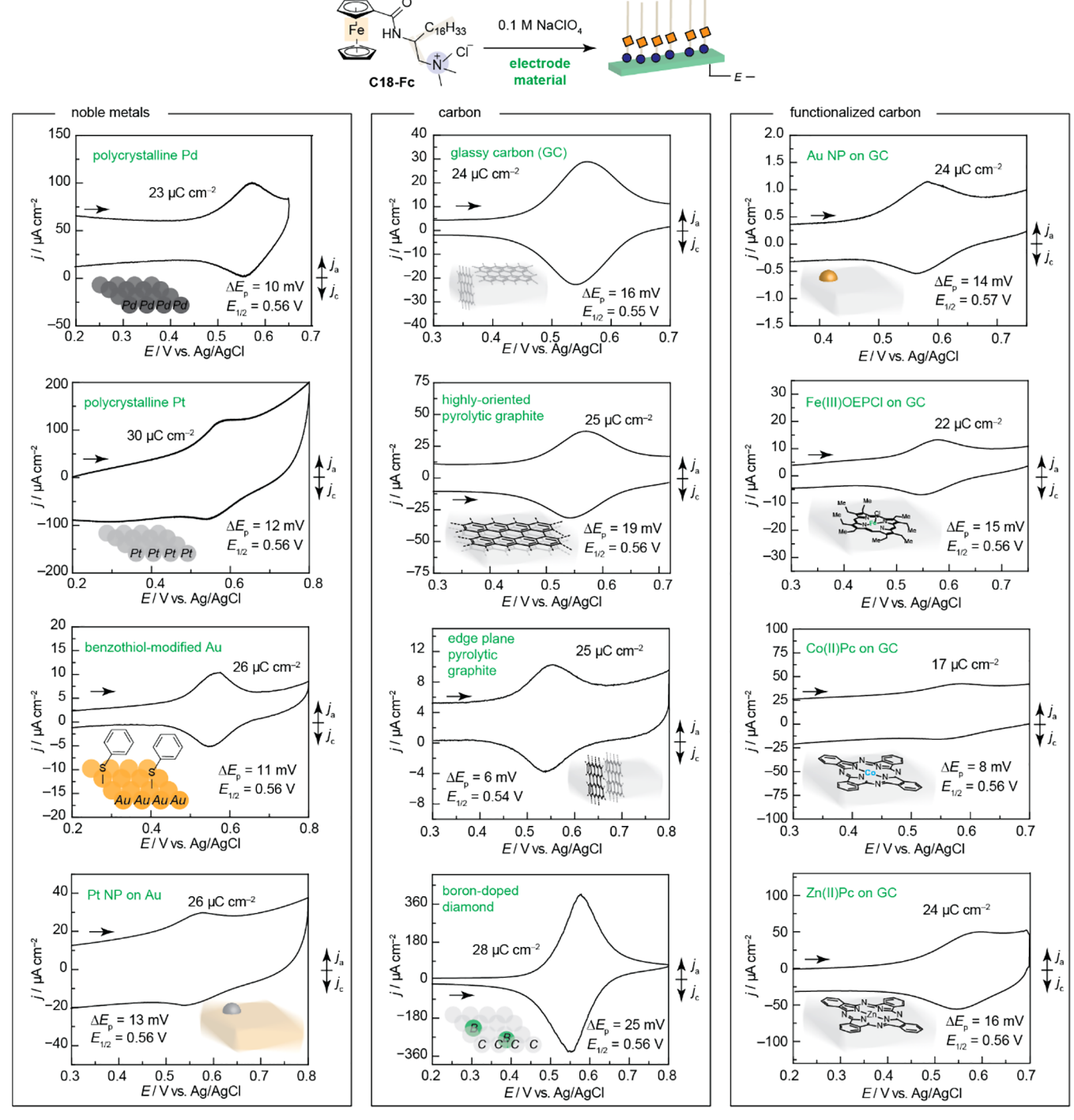


Figure 3. Electrode materials scope, i.e., electrode-orthogonality, of the self-assembled non-covalent layer. (Noble metals—top to bottom) CV of Pd disk at 100 mV s⁻¹ in 0.1 M NaClO₄ containing 200 μM C18-Fc. CV of Pt disk at 100 mV s⁻¹ in 0.1 M NaClO₄ containing 67 μM HClO₄ and 200 μM C18-Fc, pH 3.6. CV of benzenethiol-modified Au at ~0.4 surface coverage at 20 mV s⁻¹ in 0.1 M NaClO₄ containing 200 μM C18-Fc. CV of Au containing Pt nanoparticles at 1.7 nmol cm⁻² surface coverage at 20 mV s⁻¹ in 0.1 M NaClO₄ containing 200 μM C18-Fc. (Carbon—top to bottom) CV of glassy carbon foil at 100 mV s⁻¹ in 0.1 M NaClO₄ containing 135 μM C18-Fc. HOPG at 20 mV s⁻¹ in 0.1 M NaClO₄ containing 200 μM C18-Fc. CV of EPG disk at 20 mV s⁻¹ in 0.1 M NaClO₄ containing 200 μM C18-Fc. (Functionalized carbon—top to bottom). CV of AuNP-modified glassy carbon disk at ~0.3 surface coverage at 2 mV s⁻¹ in 0.1 M NaClO₄ containing 135 μM C18-Fc. CV of Fe(III)OEPCl (8 nmol cm⁻² surface coverage) adsorbed on GC at 20 mV s⁻¹ in 0.1 M NaClO₄ containing 200 μM C18-Fc. CV of Co(II)Pc (3 nmol cm⁻² surface coverage) adsorbed on GC at 100 mV s⁻¹ in 0.1 M NaClO₄ containing 200 μM C18-Fc. CV of Zn(II)Pc (0.5 nmol cm⁻² surface coverage) adsorbed on GC at 100 mV s⁻¹ in 0.1 M NaClO₄ containing 200 μM C18-Fc. All experiments conducted with a positive direction of scan under N₂.

on Au in the absence of electrolyte^{77,79} as well as those reported *in situ* for Fc-terminated alkane thiol monolayers.^{52,81} We observe a rise at 1625 cm^{-1} , which does not shift in D_2O_1

Figure S16. The peak position is in line with the carbonyl stretching frequency for amides, ^{82,83} and thus, we assign the band to the ν (CO) of the amide linkage. A rise at 1535 cm⁻¹ is

observed, which significantly shifts in D₂O (1535 to 1422 cm⁻¹, Figure S16). Together with the computational estimation for the $\delta(NH)$ in C18-Fc (Figure S17, 1547 cm⁻¹), we assign this feature to the δ (NH) of the amide. We observe a rise at 1479 cm⁻¹, which is present in D₂O (Figure S16). This value is in line with the literature-reported values for both $\delta(CH_2)$ of the aliphatic tail and the $\nu(Fe-C)$ stretching mode of the Fc. 63,78,81,84 We observe a rise at 1110 cm⁻¹. This peak is assigned to the perchlorate anion. ⁶³ Taken together, our absolute spectroscopic observations show that C18-Fc forms a molecular layer, repelling interfacial water with a significant population of the ammonium head group pointing towards the surface and the Fc oriented with the Fe-C axis primarily perpendicular to the surface, Scheme 3 (left, bottom). We note, however, that our data do not rule out structural disorder in the aliphatic tail region, e.g., the tails can be tilted in various directions to produce domains of dense and sparse aliphatic grouping. As the OCV of the system in the absence of C18-Fc is lower than the potential of zero free charge of Au (-0.011 to 0.336 V,85-87 range quoted for predominant low index facets of Au present in SEIRAS-active films (4), we rationalize that the non-covalent electrostatic interactions between the negatively charged Au electrode and the positively charged ammonium cations electrostatically template the layer assembly on the timescale of the CV experiment. Similarly, the presence of a perchlorate signal upon C18-Fc addition at the OCV suggests that the counterion is not fully replaced by the negatively charged interface, further supporting structural disorder in the layer.

The potential-dependent changes to the C18-Fc spectroscopic features demonstrate that the layer remains intact during Fc redox, mimicking features reported for the analogous covalently bound ferrocene. To accentuate the differences in the spectroscopic changes as a function of the applied potential, the relative spectra are reported in Figure 2b. We observe that as Fc is oxidized, Figure 2c, the feature assigned to ClO₄⁻ increases, Figure 2d, blue. This observation suggests that ClO₄ is sequestered from the bulk solution to ion pair with the oxidized C18-Fc, similar to previous observations for Fc covalently bound to an Au surface. ^{63,66,88} The peak assigned to the $\nu(CO)$ decreases in favor of a new feature centered at 1665 cm⁻¹ (Figures 2b,e, blue). We hypothesize that the blueshift is due to the oxidation of the Fc, as we would expect the conjugated amide CO bond to contract,⁵² and identical features are observed in D₂O (Figures S16, S18, and S19). We observe a new feature at 3100 cm⁻¹ (Figures 2b,f), coincident with Fc oxidation, Figure 2c. This feature is also observed in D₂O (Figures S16, S18, and S19) and is in line with the wavenumber reported for $\nu({\rm CH})$ of the Fc cyclopentadienyl ring. 52,63,81,84,89,90 These results demonstrate that Fc oxidation induces a structural change that favors the cyclopentadienyl rings to orient perpendicular to the interface, Scheme 3, right. Interestingly, this structural change has also been invoked for ferrocene alkyl thiols *covalently* bound to Au upon oxidation. ^{63,78,81,84,88} We observe a rise in the peak assigned to the $\delta(NH)$, Figure 2b,g, blue. As Fc is oxidized, this peak exchanges in favor of a peak centered at 1549 cm⁻¹. We hypothesize that the observed blueshift from 1535 to 1549 cm⁻¹ arises due to the shortening of the bonds conjugated to the cyclopentadienyl rings. We observe a rise in the features corresponding to the aliphatic tail and ammonium head group, Figure 2b,h. This combined signal intensity increases as Fc is oxidized but persists as the applied potential switches to the

negative direction (Figure 2h, red). This observation suggests that as the Fc is oxidized, the alkyl tails tilt away from the surface normal, Scheme 3, right. We hypothesize that since the Fc is embedded inside the alkyl chain, the sequestration of ${\rm ClO_4}^-$ as an ion-pairing partner from the bulk solution results in a global tilt of the alkyl chain as well as an orientation change of the Fc $^+$ unit relative to the electrode surface normal to accommodate the anion. Together, these results demonstrate that upon Fc oxidation, the C-N of the amide twists to favor a high surface population of Fc $^+$ parallel to the surface, accompanied by ion-pairing with ${\rm ClO_4}^-$ and a global tilt of the C18-Fc moiety relative to the surface normal.

Comparison of the first scan for the self-assembled C18-Fc layer with the second subsequent scan shows the convergence of the self-assembled interfacial structure (see Figures S20 and S21). Importantly, SEIRAS experiments conducted in the presence of C2-Fc do not reveal any significant spectroscopic changes (Figure S22), showing that layer formation is not observed for the freely diffusing C2-Fc control. This result is consistent with a structural model in which the secondary hydrophobic interaction between neighboring C18-Fc serves to establish a layer of C18-Fc at the Au interface. Without these non-covalent interactions, co-localization does not occur. We note that our conclusions lie in contrast to those in the literature that suggest that the ammonium head group is electrostatically repelled from the electrochemical interface at positive potentials. 43,44,91 Thus, we reason, after the initial templating via electrostatic interactions between the ammonium head group and the Au surface, the secondary hydrophobic interactions between C18-Fc monomers enable the layer to persist at potential values far more positive than the PZFC, Scheme 3, right, on the timescale of the CV experiment.

Non-Covalent Design Enables Molecular Layer to Self-Assemble at a Variety of Materials, i.e., via an **Electrode-Orthogonal Process.** As our mechanism for C18-Fc layer formation at the Au electrode interface involves the combined non-covalent interactions of electrostatics and hydrophobics, we envisioned that the layers would form over a wide array of different electrode materials. Figure 3 demonstrates this electrode-orthogonality. For all electrode materials, we observe $17-30 \mu C \text{ cm}^{-2}$ of charge passed for the C18-Fc oxidation, consistent with monolayer formation (see above), albeit at slightly different concentrations of bulk C18-Fc. In addition, for all electrode materials, the anodic and cathodic C18-Fc redox features are less than 25 mV, inconsistent with solution-dissolved one-electron redox and consistent with an immobilized Fc redox species. Furthermore, for all materials, the $E_{1/2}$ of the layers ($E_{1/2}$ 0.54 to 0.57 V) are nearly identical to what we observe on Au, see above, demonstrating that the ~120 mV positive shift relative to C2-Fc is retained on all materials examined. The observation that the electrochemical features diagnostic of a self-assembled layer persists across a wide range of materials suggests that the PZFC values of all electrodes examined are negative of the C18-Fc $E_{1/2}$ value. Indeed, for well-characterized Au, Pt, and Pd materials, the observed $E_{1/2}$ of C18-Fc is more positive than the reported PZFC ranges at -0.011 to 0.336~V, 85,86 0.031 to 0.101 V, $^{92-96}$ and -0.075 to 0.101 V, $^{97-99}$ respectively. Together, these results suggest that the C18-Fc forms nearly identical structures to what we characterized on Au.

The self-assembled layer forms on modified polycrystalline transition-metal materials, Figure 3, left column. The layer

forms on Pd and Pt electrodes. We note that, for Pt, surface oxides form at potential values competitive with the C18-Fc redox feature under the neutral pH conditions examined. We found that the C18-Fc redox feature can be revealed by acidifying the electrolyte solution as the Fc redox process is pH-independent, whereas the oxide feature is sensitive to the pH. As we use the Fc redox wave to probe the success of selfassembled layer formation, we are unable to determine if electrode materials that competitively corrode or form surface oxides are compatible. The layer forms on modified Au materials containing ~45% surface coverage of organic modifiers 100 (Figure S23). The layer also forms on composite electrodes, such as Pt nanoparticles on Au (1.7 nmol cm⁻² surface coverage, Figure S24). Together, we show that the noncovalent self-assembled layers form on common transitionmetal electrodes that do not form competitive oxide layers or corrode, despite the variation in surface morphologies and functionalization.

The self-assembled layer forms on functionalized and unfunctionalized carbon materials, Figure 3, middle and right columns. The layer is insensitive to the predominant surfacetermination of carbon. The layer forms on glassy carbon, highly oriented pyrolytic graphite (HOPG), edge-plate pyrolytic graphite (EPG), and boron-doped diamond electrodes (BDD). We note, for the BDD, charge integration reflective of layer formation was only possible at scan rates >1 V/s, which could suggest multilayer formation on this electrode. The layer forms on carbon materials modified with Au nanoparticles (30% surface coverage, Figure S25). Finally, composite glassy carbon electrodes modified with well-utilized heterogeneous catalysts, 101-103 such as iron (III) octaethylporphyrin chloride (FeOEPCl, surface coverage, 8 nmol cm⁻², Figure S26 and Table S7), cobalt phthalocyanine (CoPc, surface coverage 3 nmol cm⁻², Figure S27 and Table S7), and the control compound, zinc phthalocyanine (ZnPc, surface coverage 0.5 nmol cm⁻², Figure S28 and Table S7), also exhibit redox features of C18-Fc consistent with self-assembled layer formation. Together, these results show the broad scope and electrode-orthogonality of our newly discovered C18-Fc self-assembled layers on electrode materials of contemporary

The wide scope of electrode materials enables the investigation of the stability limits of the C18-Fc selfassembled layer using electrodes with wide potential windows. Among the materials investigated, glassy carbon has the widest potential window. Figures 4 and S29 depict that the layer formed on glassy carbon remains intact with a nearly constant integrated charge over a 2.9 V window. We note that SEIRA data taken over this identical expanded potential range on Au surfaces exhibit minimal changes to the observed spectroscopic features (see Figure S30 and Table S8), consistent with the potential-dependent stability observed for the proposed C18-Fc self-assembled layer on glassy carbon surfaces in Figure 4. This window is larger than the documented values for thiol (-1.1 to 0.95 V), ^{18,21} N-heterocyclic carbene (-0.4 to 0.6 V)V), 21 and isocyanide (-1.15 to 0.95 V) 19,22 modifications, as well as non-covalent immobilization strategies such as pyrene $\pi - \pi$ stacking on carbon (-2.1 to 0.5 V). ^{25,33} We note that the potential stability window of the C18-Fc self-assembled layer is probed in the presence of C18-Fc in bulk solution. Thus, while the requirement to have C18-Fc present in the bulk solution limits the layer's ex situ applications, under electrochemical conditions, provided that the synthesized amphiphile is soluble

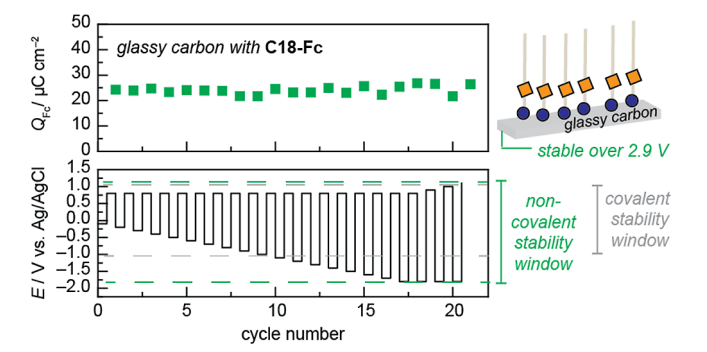


Figure 4. Stability of C18-Fc layer on a glassy carbon electrode as a function of the applied potential. (top) Charge integration of C18-Fc oxidative wave as a function of (bottom) cyclic voltammogram cycle number with gradually expanding potential window range. The experiment was conducted in 0.1 M NaClO₄ containing 135 μM C18-Fc. The stability range observed is indicated with green dashed lines. Gray dashed lines summarize literature-reported potential-dependent stability ranges for covalent modifications described in the main text.

in the electrolyte of interest and does not degrade in the bulk solution, we show that the self-assembled layer is maintained in diverse electrochemical environments (e.g., applied potential, varying electrode materials).

CONCLUSIONS

In this work, we synthesize a series of ammonium-based amphiphilic molecules with appended ferrocene redox probes and investigate their voltammetric response and in situ infrared spectra at Au surfaces. Our data mimic those reported for analogous covalently bound ferrocene to Au and are consistent with the formation of an in situ self-assembling molecular layer of amphiphiles at the electrified surface that is driven by combined non-covalent electrostatic and van der Waals interactions. Critically, the latter non-covalent interaction enables the layer to remain intact even at applied potential values where electrostatic repulsion should repel the layer. In contrast to covalent systems, the self-assembled non-covalent layer is reversible, i.e., it is easily rinsed off with water, and is independent of the surface chemistry of the electrode material. This non-fouling property of the layer enables the electrodeorthogonality of self-assembly; micromolar concentrations of the amphiphile in bulk solution allow for modification of a variety of electrode materials, enabling its application to electrochemical systems without competitive potential-dependent linkage degradation. Thus, our mechanistic finding enables us to produce self-assembled electrode-orthogonal layers at electrode interfaces, mimicking covalent molecular tuning over a wide range of electrode materials and an expanded potential range.

In all, the non-covalent strategy hijacks the atomistic precision inherent to ex situ organic synthesis of amphiphiles with in situ non-covalent self-assembly. We anticipate that this generalizable strategy will impact the design of new hybrid architectures, including the localization of a diverse array of redox-active moieties beyond Fc, to fine-tune charge transfer at emerging electrode materials for applications in energy storage and conversion, molecular sensing, and electro-organic synthesis.

ASSOCIATED CONTENT

Supporting Information

The Supporting Information is available free of charge at https://pubs.acs.org/doi/10.1021/jacs.3c04387.

Experimental and computational details and methods; synthetic procedures; electrochemical data; in situ spectroscopic data; dynamic light scattering data; quantum chemical calculations; NMR data; HRMS data (PDF)

AUTHOR INFORMATION

Corresponding Author

Anna Wuttig — Department of Chemistry, University of Chicago, Chicago, Illinois 60637, United States; orcid.org/0000-0002-5552-0981; Email: awuttig@uchicago.edu

Authors

Deepak Badgurjar — Department of Chemistry, University of Chicago, Chicago, Illinois 60637, United States Madison Huynh — Department of Chemistry, University of Chicago, Chicago, Illinois 60637, United States Benjamin Masters — Department of Chemistry, University of Chicago, Chicago, Illinois 60637, United States

Complete contact information is available at: https://pubs.acs.org/10.1021/jacs.3c04387

Author Contributions

[†]D.B. and M.H. contributed equally to this work.

Notes

The authors declare no competing financial interest.

ACKNOWLEDGMENTS

The authors thank the research laboratories of Professors John Anderson, Stuart Rowan, Chong Liu, Scott Snyder, Michael Hopkins, and Viresh Rawal for sharing their chemical inventories. The authors thank Professor Stephen Maldonado for pointing out reference 50. This research made use of the University of Chicago Mass Spectrometry Facility (NSF instrumentation grant CHE-1048528). This work made use of the shared facilities at the University of Chicago Materials Research Science and Engineering Center, supported by the National Science Foundation under award number DMR-2011854. Computing resources were provided by the Research Computing Center at the University of Chicago. Parts of this work were carried out at the Soft Matter Characterization Facility of the University of Chicago. The authors thank Professor Stuart Rowan for the use of the density meter. This research was supported by the University of Chicago startup funds as well as a Neubauer Family Assistant Professorship to A.W. (University of Chicago). Acknowledgment is made to the donors of the American Chemical Society Petroleum Research Fund for partial support of this research. The authors thank Dr. Karen M. Watters for scientific editing of the manuscript.

REFERENCES

(1) Nuzzo, R. G.; Allara, D. L. Adsorption of Bifunctional Organic Disulfides on Gold Surfaces. *J. Am. Chem. Soc.* **1983**, *105*, 4481–4483. (2) Bain, C. D.; Whitesides, G. M. Molecular-Level Control over Surface Order in Self-Assembled Monolayer Films of Thiols on Gold. *Science* **1988**, *240*, 62–63.

- (3) Sellers, H.; Ulman, A.; Shnidman, Y.; Eilers, J. E. Structure and Binding of Alkanethiolates on Gold and Silver Surfaces: Implications for Self-Assembled Monolayers. *J. Am. Chem. Soc.* **1993**, *115*, 9389–9401.
- (4) Kelley, S. O.; Barton, J. K.; Jackson, N. M.; Hill, M. G. Electrochemistry of Methylene Blue Bound to a DNA-Modified Electrode. *Bioconjugate Chem.* **1997**, *8*, 31–37.
- (5) Nano, A.; Furst, A. L.; Hill, M. G.; Barton, J. K. DNA Electrochemistry: Charge-Transport Pathways through DNA Films on Gold. *J. Am. Chem. Soc.* **2021**, *143*, 11631–11640.
- (6) Smith, C. P.; White, H. S. Voltammetry of Molecular Films Containing Acid/Base Groups. *Langmuir* **1993**, *9*, 1–3.
- (7) White, H. S.; Peterson, J. D.; Cui, Q.; Stevenson, K. J. Voltammetric Measurement of Interfacial Acid/Base Reactions. *J. Phys. Chem. B* **1998**, *102*, 2930–2934.
- (8) Delley, M. F.; Nichols, E. M.; Mayer, J. M. Interfacial Acid-Base Equilibria and Electric Fields Concurrently Probed by *In Situ* Surface-Enhanced Infrared Spectroscopy. *J. Am. Chem. Soc.* **2021**, *143*, 10778–10792.
- (9) Chidsey, C. E. D. Free Energy and Temperature Dependence of Electron Transfer at the Metal-Electrolyte Interface. *Science* **1991**, 251, 919–922.
- (10) Tender, L.; Carter, M. T.; Murray, R. W. Cyclic Voltammetric Analysis of Ferrocene Alkanethiol Monolayer Electrode Kinetics Based on Marcus Theory. *Anal. Chem.* **1994**, *66*, 3173–3181.
- (11) Fang, Y.; Flake, J. C. Electrochemical Reduction of CO₂ at Functionalized Au Electrodes. *J. Am. Chem. Soc.* **2017**, *139*, 3399–3405.
- (12) Cao, Z.; Zacate, S. B.; Sun, X.; Liu, J.; Hale, E. M.; Carson, W. P.; Tyndall, S. B.; Xu, J.; Liu, X.; Liu, X.; et al. Tuning Gold Nanoparticles with Chelating Ligands for Highly Efficient Electrocatalytic CO₂ Reduction. *Angew. Chem., Int. Ed.* **2018**, *57*, 12675–12679.
- (13) Sévery, L.; Szczerbiński, J.; Taskin, M.; Tuncay, I.; Brandalise Nunes, F.; Cignarella, C.; Tocci, G.; Blacque, O.; Osterwalder, J.; Zenobi, R.; et al. Immobilization of Molecular Catalysts on Electrode Surfaces Using Host–Guest Interactions. *Nat. Chem.* **2021**, *13*, 523–529.
- (14) Hickman, J. J.; Laibinis, P. E.; Auerbach, D. I.; Zou, C.; Gardner, T. J.; Whitesides, G. M.; Wrighton, M. S. Toward Orthogonal Self-Assembly of Redox Active Molecules on Platinum and Gold: Selective Reaction of Disulfide with Gold and Isocyanide with Platinum. *Langmuir* 1992, 8, 357–359.
- (15) Love, J. C.; Estroff, L. A.; Kriebel, J. K.; Nuzzo, R. G.; Whitesides, G. M. Self-Assembled Monolayers of Thiolates on Metals as a Form of Nanotechnology. *Chem. Rev.* **2005**, *105*, 1103–1169.
- (16) Edwards, G. A.; Bergren, A. J.; Porter, M. D. Chemically Modified Electrodes. In *Handbook of Electrochemistry*; Elsevier, 2007; pp 295–327.
- (17) Amit, E.; Dery, L.; Dery, S.; Kim, S.; Roy, A.; Hu, Q.; Gutkin, V.; Eisenberg, H.; Stein, T.; Mandler, D.; et al. Electrochemical Deposition of N-Heterocyclic Carbene Monolayers on Metal Surfaces. *Nat. Commun.* **2020**, *11*, 5714.
- (18) Widrig, C. A.; Chung, C.; Porter, M. D. The Electrochemical Desorption of N-Alkanethiol Monolayers from Polycrystalline Au and Ag Electrodes. *J. Electroanal. Chem.* **1991**, *310*, 335–359.
- (19) Horswell, S. L.; O'Neil, I. A.; Schiffrin, D. J. Potential Modulated Infrared Reflectance Spectroscopy of Pt-Diisocyanide Nanostructured Electrodes. *J. Phys. Chem. B* **2001**, *105*, 941–947.
- (20) Pensa, E.; Vericat, C.; Grumelli, D.; Salvarezza, R. C.; Park, S. H.; Longo, G. S.; Szleifer, I.; Méndez De Leo, L. P. New Insight into the Electrochemical Desorption of Alkanethiol SAMs on Gold. *Phys. Chem. Chem. Phys.* **2012**, *14*, 12355–12367.
- (21) Crudden, C. M.; Horton, J. H.; Ebralidze, I. I.; Zenkina, O. V.; McLean, A. B.; Drevniok, B.; She, Z.; Kraatz, H. B.; Mosey, N. J.; Seki, T.; et al. Ultra Stable Self-Assembled Monolayers of N-Heterocyclic Carbenes on Gold. *Nat. Chem.* **2014**, *6*, 409–414.
- (22) Lee, G. L.; Chan, T.; Palasz, J. M.; Kubiak, C. P. Layer-by-Layer Deposition of Rh(I) Diisocyanide Coordination Polymers on

- Au(111) and Their Chemical and Electrochemical Stability. J. Phys. Chem. C 2022, 126, 16522–16528.
- (23) Delamar, M.; Hitmi, R.; Pinson, J.; Savéant, J. M. Covalent Modification of Carbon Surfaces by Grafting of Functionalized Aryl Radicals Produced from Electrochemical Reduction of Diazonium Salts. J. Am. Chem. Soc. 1992, 114, 5883–5884.
- (24) Allongue, P.; Delamar, M.; Desbat, B.; Fagebaume, O.; Hitmi, R.; Pinson, J.; Savéant, J. M. Covalent Modification of Carbon Surfaces by Aryl Radicals Generated from the Electrochemical Reduction of Diazonium Salts. J. Am. Chem. Soc. 1997, 119, 201–207.
- (25) Blakemore, J. D.; Gupta, A.; Warren, J. J.; Brunschwig, B. S.; Gray, H. B. Noncovalent Immobilization of Electrocatalysts on Carbon Electrodes for Fuel Production. *J. Am. Chem. Soc.* **2013**, *135*, 18288–18291.
- (26) Lionetti, D.; Day, V. W.; Blakemore, J. D. Noncovalent Immobilization and Surface Characterization of Lanthanide Complexes on Carbon Electrodes. *Dalton Trans.* **2017**, *46*, 11779–11789.
- (27) Reuillard, B.; Ly, K. H.; Rosser, T. E.; Kuehnel, M. F.; Zebger, I.; Reisner, E. Tuning Product Selectivity for Aqueous CO₂ Reduction with a Mn(Bipyridine)-Pyrene Catalyst Immobilized on a Carbon Nanotube Electrode. *J. Am. Chem. Soc.* **2017**, *139*, 14425–14435.
- (28) Ruiz-Botella, S.; Peris, E. Immobilization of Pyrene-Adorned N-Heterocyclic Carbene Complexes of Rhodium(I) on Reduced Graphene Oxide and Study of Their Catalytic Activity. *ChemCatChem* **2018**, *10*, 1874–1881.
- (29) Sinha, S.; Sonea, A.; Shen, W.; Hanson, S. S.; Warren, J. J. Heterogeneous Aqueous CO_2 Reduction Using a Pyrene-Modified Rhenium(I) Diimine Complex. *Inorg. Chem.* **2019**, 58, 10454–10461.
- (30) Rusling, J. F.; Shi, C. N.; Gosser, D. K.; Shukla, S. S. Electrocatalytic Reactions in Organized Assemblies: Part I. Reduction of 4-Bromobiphenyl in Cationic and Non-Ionic Micelles. *J. Electroanal. Chem.* **1988**, 240, 201–216.
- (31) Pinson, J.; Podvorica, F. Attachment of Organic Layers to Conductive or Semiconductive Surfaces by Reduction of Diazonium Salts. *Chem. Soc. Rev.* **2005**, *34*, 429–439.
- (32) Le Goff, A.; Reuillard, B.; Cosnier, S. A Pyrene-Substituted Tris(Bipyridine)Osmium(II) Complex as a Versatile Redox Probe for Characterizing and Functionalizing Carbon Nanotube- and Graphene-Based Electrodes. *Langmuir* 2013, 29, 8736–8742.
- (33) Kohmoto, M.; Ozawa, H.; Yang, L.; Hagio, T.; Matsunaga, M.; Haga, M. A. Controlling the Adsorption of Ruthenium Complexes on Carbon Surfaces through Noncovalent Bonding with Pyrene Anchors: An Electrochemical Study. *Langmuir* **2016**, 32, 4141–4152.
- (34) Kamau, G. N.; Rusling, J. F. Electrocatalytic Reactions in Organized Assemblies: Part III. Reduction of Allyl Halides by Bipyridyl Derivatives of Cobalt in Anionic and Cationic Micelles. *J. Electroanal. Chem.* **1988**, 240, 217–226.
- (35) Owlia, A.; Wang, Z.; Rusling, J. F. Electrochemistry and Electrocatalysis with Vitamin B_{12} in an AOT Water-in-Oil Microemulsion. *J. Am. Chem. Soc.* **1989**, *111*, 5091–5098.
- (36) Rusling, J. F. Controlling Electrochemical Catalysis with Surfactant Microstructures. *Acc. Chem. Res.* **1991**, *24*, 75–81.
- (37) Rusling, J. F. Electrochemistry and Electrochemical Catalysis in Microemulsions. In *Modern Aspects of Electrochemistry*; Springer: Boston, MA, 1994; pp 49–104.
- (38) Kodama, Y.; Imoto, M.; Ohta, N.; Kitani, A.; Ito, S. Control of Product Distribution by Use of Surfactants in Cathodic Reduction of Acetophenone. *Chem. Lett.* **1997**, *26*, 337–338.
- (39) Rusling, J. F. Molecular Aspects of Electron Transfer at Electrodes in Micellar Solutions. *Colloids Surf., A* 1997, 123–124, 81–88.
- (40) Carrero, H.; Gao, J.; Rusling, J. F.; Lee, C. W.; Fry, A. J. Direct and Catalyzed Electrochemical Syntheses in Microemulsions. *Electrochim. Acta* **1999**, *45*, 503–512.
- (41) Ahmadi, M. F.; Rusling, J. F. Fluorescence Probe Spectroelectrochemistry at Silver Electrodes in Dimethylformamide and Aqueous Hexadecyltrimethylammonium Chloride. *Langmuir* **1991**, *7*, 1529–1536.

- (42) Abbott, A. P.; Gounili, G.; Bobbitt, J. M.; Rusling, J. F.; Kumosinski, T. F. Electron Transfer between Amphiphilic Ferrocenes and Electrodes in Cationic Micellar Solution. *J. Phys. Chem.* **1992**, *96*, 11091–11095.
- (43) Zhang, Z. Q.; Banerjee, S.; Thoi, V. S.; Hall, A. S. Reorganization of Interfacial Water by an Amphiphilic Cationic Surfactant Promotes CO₂ Reduction. *J. Phys. Chem. Lett.* **2020**, *11*, 5457–5463.
- (44) Ge, W.; Chen, Y.; Fan, Y.; Zhu, Y.; Liu, H.; Song, L.; Liu, Z.; Lian, C.; Jiang, H.; Li, C. Dynamically Formed Surfactant Assembly at the Electrified Electrode-Electrolyte Interface Boosting CO₂ Electroreduction. *J. Am. Chem. Soc.* **2022**, *144*, 6613–6622.
- (45) Pennathur, A. K.; Tseng, C.; Salazar, N.; Dawlaty, J. M. Controlling Water Delivery to an Electrochemical Interface with Surfactants. J. Am. Chem. Soc. 2023, 145, 2421–2429.
- (46) Creager, S. E.; Rowe, G. K. Redox Properties of Ferrocenylalkane Thiols Coadsorbed with Linear N-Alkanethiols on Polycrystalline Bulk Gold Electrodes. *Anal. Chim. Acta* **1991**, 246, 233–239.
- (47) Rowe, G. K.; Creager, S. E. Redox and Ion-Pairing Thermodynamics in Self-Assembled Monolayers. *Langmuir* **1991**, *7*, 2307–2312.
- (48) Valincius, G.; Niaura, G.; Kazakevičienė, B.; Talaikytė, Z.; Kažemėkaitė, M.; Butkus, E.; Razumas, V. Anion Effect on Mediated Electron Transfer through Ferrocene-Terminated Self-Assembled Monolayers. *Langmuir* **2004**, *20*, 6631–6638.
- (49) Savéant, J.-M.; Costentin, C. Elements of Molecular and Biomolecular Electrochemistry: An Electrochemical Approach to Electron Transfer Chemistry, 2nd ed.; John Wiley & Sons, 2019.
- (50) Smith, C. P.; White, H. S. Theory of the Interfacial Potential Distribution and Reversible Voltammetric Response of Electrodes Coated with Electroactive Molecular Films. *Anal. Chem.* **1992**, *64*, 2398–2405.
- (51) Duffin, T. J.; Nerngchamnong, N.; Thompson, D.; Nijhuis, C. A. Direct Measurement of the Local Field within Alkyl-Ferrocenyl-Alkanethiolate Monolayers: Importance of the Supramolecular and Electronic Structure on the Voltammetric Response and Potential Profile. *Electrochim. Acta* **2019**, *311*, 92–102.
- (52) Popenoe, D. D.; Deinhammer, R. S.; Porter, M. D. Infrared Spectroelectrochemical Characterization of Ferrocene-Terminated Alkanethiolate Monolayers at Gold. *Langmuir* 1992, 8, 2521–2530.
- (53) Saji, T.; Hoshino, K.; Aoyagui, S. Reversible Formation and Disruption of Micelles by Control of the Redox State of the Head Group. *J. Am. Chem. Soc.* **1985**, *107*, 6865–6868.
- (54) Bard, A. J.; Faulkner, L. R.; White, H. S. *Electrochemical Methods: Fundamentals and Applications*, 3rd ed.; John Wiley & Sons Ltd: Hoboken, NJ, 2022.
- (55) Nerngchamnong, N.; Thompson, D.; Cao, L.; Yuan, L.; Jiang, L.; Roemer, M.; Nijhuis, C. A. Nonideal Electrochemical Behavior of Ferrocenyl-Alkanethiolate SAMs Maps the Microenvironment of the Redox Unit. *J. Phys. Chem. C* **2015**, *119*, 21978–21991.
- (56) Patel, D. A.; Weller, A. M.; Chevalier, R. B.; Karos, C. A.; Landis, E. C. Ordering and Defects in Self-Assembled Monolayers on Nanoporous Gold. *Appl. Surf. Sci.* **2016**, *387*, 503–512.
- (57) Dionne, E. R.; Dip, C.; Toader, V.; Badia, A. Micromechanical Redox Actuation by Self-Assembled Monolayers of Ferrocenylalkanethiolates: Evens Push More Than Odds. *J. Am. Chem. Soc.* **2018**, 140, 10063–10066.
- (58) Jangid, V.; Brunel, D.; Sanchez-Adaime, E.; Bharwal, A. K.; Dumur, F.; Duché, D.; Abel, M.; Koudia, M.; Buffeteau, T.; Nijhuis, C. A.; et al. Improving Orientation, Packing Density, and Molecular Arrangement in Self-Assembled Monolayers of Bianchoring Ferrocene-Triazole Derivatives by "Click" Chemistry. *Langmuir* **2022**, 38, 3585–3596.
- (59) Kobayashi, Y.; Yokota, Y.; Wong, R. A.; Hong, M.; Takeya, J.; Osawa, S.; Ishiwari, F.; Shoji, Y.; Harimoto, T.; Sugimoto, K.; et al. Single-Molecule Observation of Redox Reactions Enabled by Rigid and Isolated Tripodal Molecules. *J. Phys. Chem. C* **2023**, *127*, 746–758.

- (60) Smalley, J. F.; Feldberg, S. W.; Chidsey, C. E. D.; Linford, M. R.; Newton, M. D.; Liu, Y. P. The Kinetics of Electron Transfer through Ferrocene-Terminated Alkanethiol Monolayers on Gold. *J. Phys. Chem. B* **1995**, *99*, 13141–13149.
- (61) Kakiuchi, T.; Iida, M.; Imabayashi, S. I.; Niki, K. Double-Layer-Capacitance Titration of Self-Assembled Monolayers of ω-Functionalized Alkanethiols on Au(111) Surface. *Langmuir* **2000**, *16*, 5397–5401.
- (62) Chidsey, C. E. D.; Bertozzi, C. R.; Putvinski, T. M.; Mujsce, A. M. Coadsorption of Ferrocene-Terminated and Unsubstituted Alkanethiols on Gold: Electroactive Self-Assembled Monolayers. *J. Am. Chem. Soc.* **1990**, *112*, 4301–4306.
- (63) Rudnev, A. V.; Zhumaev, U.; Utsunomiya, T.; Fan, C.; Yokota, Y.; Fukui, K.-i.; Wandlowski, T. Ferrocene-Terminated Alkanethiol Self-Assembled Monolayers: An Electrochemical and *In Situ* Surface-Enhanced Infra-Red Absorption Spectroscopy Study. *Electrochim. Acta* 2013, 107, 33–44.
- (64) Rudnev, A. V.; Yoshida, K.; Wandlowski, T. Electrochemical Characterization of Self-Assembled Ferrocene-Terminated Alkanethiol Monolayers on Low-Index Gold Single Crystal Electrodes. *Electrochim. Acta* **2013**, *87*, 770–778.
- (65) Stragliotto, M. F.; Fernández, J. L.; Dassie, S. A.; Giacomelli, C. E. An Integrated Experimental-Theoretical Approach to Understand the Electron Transfer Mechanism of Adsorbed Ferrocene-Terminated Alkanethiol Monolayers. *Electrochim. Acta* **2018**, 265, 303–315.
- (66) Wong, R. A.; Yokota, Y.; Wakisaka, M.; Inukai, J.; Kim, Y. Probing Consequences of Anion-Dictated Electrochemistry on the Electrode/Monolayer/Electrolyte Interfacial Properties. *Nat. Commun.* **2020**, *11*, 4194.
- (67) Seiler, P.; Dunitz, J. D. A New Interpretation of the Disordered Crystal Structure of Ferrocene. *Acta Crystallogr., Sect. B: Struct. Crystallogr. Cryst. Chem.* 1979, 35, 1068–1074.
- (68) Manne, S.; Cleveland, J. P.; Gaub, H. E.; Stucky, G. D.; Hansma, P. K. Direct Visualization of Surfactant Hemimicelles by Force Microscopy of the Electrical Double Layer. *Langmuir* **1994**, *10*, 4409–4413.
- (69) Paria, S.; Khilar, K. C. A Review on Experimental Studies of Surfactant Adsorption at the Hydrophilic Solid—Water Interface. *Adv. Colloid Interface Sci.* **2004**, *110*, 75–95.
- (70) Zhang, R.; Somasundaran, P. Advances in Adsorption of Surfactants and Their Mixtures at Solid/Solution Interfaces. *Adv. Colloid Interface Sci.* **2006**, 123–126, 213–229.
- (71) Osawa, M. Dynamic Processes in Electrochemical Reactions Studied by Surface-Enhanced Infrared Absorption Spectroscopy (SEIRAS). *Bull. Chem. Soc. Jpn.* **1997**, *70*, 2861–2880.
- (72) Osawa, M. In-Situ Surface-Enhanced Infrared Spectroscopy of the Electrode/Solution Interface. In Diffraction and Spectroscopic Methods in Electrochemistry (Advances in Electrochemical Science and Engineering; Alkire, R. C.; Kolb, D. M.; Lipkowski, J.; Ross, P. N., Eds.; Wiley-VCH: New York, 2006; Vol. 9, pp 269–314.
- (73) Yaguchi, M.; Uchida, T.; Motobayashi, K.; Osawa, M. Speciation of Adsorbed Phosphate at Gold Electrodes: A Combined Surface-Enhanced Infrared Absorption Spectroscopy and DFT Study. *J. Phys. Chem. Lett.* **2016**, *7*, 3097–3102.
- (74) Wuttig, A.; Ryu, J.; Surendranath, Y. Electrolyte Competition Controls Surface Binding of CO Intermediates to CO₂ Reduction Catalysts. *J. Phys. Chem. C* **2021**, *125*, 17042–17050.
- (75) Ataka, K.-i.; Yotsuyanagi, T.; Osawa, M. Potential-Dependent Reorientation of Water Molecules at an Electrode/Electrolyte Interface Studied by Surface-Enhanced Infrared Absorption Spectroscopy. J. Phys. Chem. 1996, 100, 10664–10672.
- (76) MacPhail, R. A.; Strauss, H. L.; Snyder, R. G.; Elliger, C. A. Carbon-Hydrogen Stretching Modes and the Structure of n-Alkyl Chains. 2. Long, All-Trans Chains. *J. Phys. Chem.* **1984**, 88, 334–341.
- (77) Himmelhaus, M.; Eisert, F.; Buck, M.; Grunze, M. Self-Assembly of n-Alkanethiol Monolayers. A Study by IR-Visible Sum Frequency Spectroscopy (SFG). *J. Phys. Chem. B* **2000**, *104*, 576–584.

- (78) Viana, A. S.; Jones, A. H.; Abrantes, L. M.; Kalaji, M. Redox Induced Orientational Changes in a Series of Short Chain Ferrocenyl Alkyl Thiols Self-Assembled on Gold(111) Electrodes. *J. Electroanal. Chem.* **2001**, *500*, 290–298.
- (79) Arnold, R.; Terfort, A.; Wöll, C. Determination of Molecular Orientation in Self-Assembled Monolayers Using IR Absorption Intensities: The Importance of Grinding Effects. *Langmuir* **2001**, *17*, 4980–4989.
- (80) Viana, R. B.; da Silva, A. B. F.; Pimentel, A. S. Infrared Spectroscopy of Anionic, Cationic, and Zwitterionic Surfactants. *Adv. Phys. Chem.* **2012**, 2012, 1–14.
- (81) Ye, S.; Sato, Y.; Uosaki, K. Redox-Induced Orientation Change of a Self-Assembled Monolayer of 11-Ferrocenyl-1-Undecanethiol on a Gold Electrode Studied by *in Situ* FT-IRRAS. *Langmuir* **1997**, *13*, 3157–3161.
- (82) Afara, N.; Omanovic, S.; Asghari-Khiavi, M. Functionalization of a Gold Surface with Fibronectin (FN) Covalently Bound to Mixed Alkanethiol Self-Assembled Monolayers (SAMs): The Influence of SAM Composition on Its Physicochemical Properties and FN Surface Secondary Structure. *Thin Solid Films* **2012**, *522*, 381–389.
- (83) Kuodis, Z.; Matulaitienė, I.; Špandyreva, M.; Labanauskas, L.; Stončius, S.; Eicher-Lorka, O.; Sadzevičienė, R.; Niaura, G. Reflection Absorption Infrared Spectroscopy Characterization of SAM Formation from 8-Mercapto-N-(Phenethyl)Octanamide Thiols with Phe Ring and Amide Groups. *Molecules* **2020**, *25*, 5633.
- (84) Ye, S.; Haba, T.; Sato, Y.; Shimazu, K.; Uosaki, K. Coverage Dependent Behavior of Redox Reaction Induced Structure Change and Mass Transport at an 11-Ferrocenyl-1-Undecanethiol Self-Assembled Monolayer on a Gold Electrode Studied by an *Insitu* IRRAS–EQCM Combined System. *Phys. Chem. Chem. Phys.* 1999, 1, 3653–3659.
- (85) Kolb, D. M.; Schneider, J. Surface Reconstruction in Electrochemistry: $Au(100-(5\times20), Au(111)-(1\times23))$ and $Au(110)-(1\times2)$. Electrochim. Acta 1986, 31, 929–936.
- (86) Dakkouri, A. S.; Kolb, D. M. Reconstruction of gold surfaces. In *Interfacial Electrochemistry: Theory, Experiment, and Applications*; Wieckowski, A., Ed.; CRC Press, 1999; pp 151–173.
- (87) Silva, A. F.; Martins, A. Capacitive and Voltammetric Responses from Stepped Faces of Gold. In *Interfacial Electrochemistry: Theory, Experiment, and Applications*; Wieckowski, A., Ed.; Marcel Dekker, Inc.: New York, 1999; pp 449–461.
- (88) Wong, R. A.; Yokota, Y.; Wakisaka, M.; Inukai, J.; Kim, Y. Discerning the Redox-Dependent Electronic and Interfacial Structures in Electroactive Self-Assembled Monolayers. *J. Am. Chem. Soc.* **2018**, 140, 13672–13679.
- (89) Tu, K.; Morhart, T. A.; Read, S. T.; Rosendahl, S. M.; Burgess, I. J. Probing Heterogeneity in Attenuated Total Reflection Surface-Enhanced Infrared Absorption Spectroscopy (ATR-SEIRAS) Response with Synchrotron Infrared Microspectroscopy. *Appl. Spectrosc.* **2021**, *75*, 1198–1206.
- (90) Eggers, P. K.; Da Silva, P.; Darwish, N. A.; Zhang, Y.; Tong, Y.; Ye, S.; Paddon-Row, M. N.; Gooding, J. J. Self-Assembled Monolayers Formed Using Zero Net Curvature Norbornylogous Bridges: The Influence of Potential on Molecular Orientation. *Langmuir* **2010**, *26*, 15665–15670.
- (91) Gao, X.; White, H. S.; Chen, S.; Abruña, H. D. Electric-Field-Induced Transitions of Amphiphilic Layers on Mercury Electrodes. *Langmuir* **1995**, *11*, 4554–4563.
- (92) Rizo, R.; Sitta, E.; Herrero, E.; Climent, V.; Feliu, J. M. Towards the Understanding of the Interfacial pH Scale at Pt(1 1 1) Electrodes. *Electrochim. Acta* **2015**, *162*, 138–145.
- (93) Martínez-Hincapié, R.; Climent, V.; Feliu, J. M. Peroxodisulfate Reduction as a Probe to Interfacial Charge. *Electrochem. Commun.* **2018**, *88*, 43–46.
- (94) Martínez-Hincapié, R.; Sebastián-Pascual, P.; Climent, V.; Feliu, J. M. Investigating Interfacial Parameters with Platinum Single Crystal Electrodes. *Russ. J. Electrochem.* **2017**, *53*, 227–236.
- (95) Sebastián, P.; Martínez-Hincapié, R.; Climent, V.; Feliu, J. M. Study of the Pt (111) | Electrolyte Interface in the Region Close to

- Neutral pH Solutions by the Laser Induced Temperature Jump Technique. *Electrochim. Acta* **2017**, 228, 667–676.
- (96) \bar{Xu} , P.; von Rueden, A. D.; Schimmenti, R.; Mavrikakis, M.; Suntivich, J. Optical Method for Quantifying the Potential of Zero Charge at the Platinum–Water Electrochemical Interface. *Nat. Mater.* **2023**, *22*, 503–510.
- (97) El-Aziz, A. M.; Kibler, L. A.; Kolb, D. M. The Potentials of Zero Charge of Pd(1 1 1) and Thin Pd Overlayers on Au(1 1 1). *Electrochem. Commun.* **2002**, *4*, 535–539.
- (98) Petrii, O. A. Zero Charge Potentials of Platinum Metals and Electron Work Functions (Review). *Russ. J. Electrochem.* **2013**, 49, 401–422.
- (99) Groß, A.; Sakong, S. Ab Initio Simulations of Water/Metal Interfaces. *Chem. Rev.* **2022**, *122*, 10746–10776.
- (100) Wan, L. J.; Terashima, M.; Noda, H.; Osawa, M. Molecular Orientation and Ordered Structure of Benzenethiol Adsorbed on Gold(111). *J. Phys. Chem. B* **2000**, *104*, 3563–3569.
- (101) Wang, M.; Torbensen, K.; Salvatore, D.; Ren, S.; Joulié, D.; Dumoulin, F.; Mendoza, D.; Lassalle-Kaiser, B.; Işci, U.; Berlinguette, C. P.; Robert, M. CO₂ Electrochemical Catalytic Reduction with a Highly Active Cobalt Phthalocyanine. *Nat. Commun.* **2019**, *10*, 3602.
- (102) Marshall-Roth, T.; Libretto, N. J.; Wrobel, A. T.; Anderton, K. J.; Pegis, M. L.; Ricke, N. D.; Van Voorhis, T.; Miller, J. T.; Surendranath, Y. A Pyridinic Fe-N₄ Macrocycle Models the Active Sites in Fe/N-Doped Carbon Electrocatalysts. *Nat. Commun.* 2020, 11, 5283
- (103) Chang, Q.; Liu, Y.; Lee, J. H.; Ologunagba, D.; Hwang, S.; Xie, Z.; Kattel, S.; Lee, J. H.; Chen, J. G. Metal-Coordinated Phthalocyanines as Platform Molecules for Understanding Isolated Metal Sites in the Electrochemical Reduction of CO₂. *J. Am. Chem. Soc.* **2022**, *144*, 16131–16138.